DeFall: Environment-Independent Passive Fall Detection using WiFi

Yuqian Hu, *Graduate Student Member, IEEE,* Feng Zhang, *Member, IEEE,* Chenshu Wu, *Senior Member, IEEE,* Beibei Wang, *Senior Member, IEEE,* and K. J. Ray Liu, *Fellow, IEEE*

***Abstract*—Fall is recognized as one of the most frequent accidents among elderly people. Many solutions, either wearable or non-contact, have been proposed for fall detection recently. Among them, WiFi-based non-contact approaches are gaining popularity due to the ubiquity and non-invasiveness. The existing works, however, usually rely on labor-intensive and time-consuming training before it can achieve a reasonable performance. In addition, the trained models often contain environment-specific information and thus cannot be generalized well for new environments. In this paper, we propose DeFall, a WiFi-based passive fall detection system that is independent of the environment and free of prior training in new environments. Unlike previous works, our key insight is to probe the physiological features inherently associated with human falls, i.e., the distinctive patterns of speed and acceleration during a fall. DeFall consists of an offline template-generating stage and an online decision-making stage, both taking the speed estimates as input. In the offline stage, augmented dynamic time warping (DTW) algorithms are performed to generate a representative template of the speed and acceleration patterns for a typical human fall. In the online phase, we compare the patterns of the real-time speed/acceleration estimates against the template to detect falls. To evaluate the performance of DeFall, we built a prototype using commercial WiFi devices and conducted experiments under different settings. The results demonstrate that DeFall achieves a detection rate above 95% with a false alarm lower than 1.50% under both line-of-sight (LOS) and non-LOS (NLOS) scenarios with one single pair of transceivers. Extensive comparison study verifies that DeFall can be generalized well to new environments without any new training.**

***Index Terms*—Fall detection system, channel state information, WiFi sensing, speed estimation**

I. Introduction

As the population ages worldwide, our society should take more and more arduous responsibilities to provide medical care for the elderly. Among all of the accidents in the elderly, falls represent the most frequent ones. The report from the World Health Organization (WHO) indicates that 20% - 30% of older people who fall suffer moderate to severe injuries [1]. Falls can even cause death. In all regions of the world, death rates caused by falls are the highest among adults over the age of 60 years [1].

Moreover, the damage caused by the falls is not only reflected in the immediate injury of the body, but also in all subsequent adverse effects caused by the lack of timely assistance, especially for those who live alone. Therefore, a real-time indoor fall detection system with timely and automatic alarms is highly in need, which could potentially save lives by requesting external help timely.

The great importance of fall detection has driven the development of various systems, which can be roughly divided into two categories: wearable and non-contact systems. The wearable techniques require users to wear special devices, including ECG sensors, barometric sensors, accelerometers, gyroscopes, and smartphones, etc., to track the motion of their bodies [2]–[6]. However, in addition to the potential false alarms of wearable systems, it is cumbersome and sometimes impractical to ask users especially the elder people to carry specialized sensors [7], which encourages the development of non-contact systems. The most common non-contact systems are vision-based [8]–[13]. Typically, an array of cameras, infrared sensors, or depth cameras like Kinect need to be deployed to monitor an area of interest. While high accuracy could be achieved under favored settings of good lighting condition and clear field of view, vision-based systems are limited by the visibility requirement and also bring privacy concerns, especially in some specific environments such as the bathrooms and bedrooms.

Inspired by the fact that the radio frequency (RF) signals can be altered by the propagation environment [14] [15], the concept of wireless sensing presents the opportunities of sensing human activities passively and many wireless technologies, such as Doppler radar and WiFi signals have been explored [16]–[23] to detect falls. However, the existing RF-based approaches either have limited coverage or require re-training in new environments, which is impractical in commercial indoor fall detection systems. We compare different types of RF-based systems in detail in Section II.

To address this issue, in this work we propose DeFall, a WiFi-based robust and environment-independent fall detection system. The key insight that sets apart DeFall from prior works is the exploitation of the physiological patterns of body speed and accelerations, rather than less explainable data-driven features used previously. Noticing that human falls experience different speed/acceleration from other daily activities, we propose to utilize the unique patterns of speed and acceleration to recognize falls. Recent work [24] has shown the feasibility to extract speed information passively from WiFi signals even in non-line-of-sight (NLOS) environments, which allows us to build DeFall upon the WiFi-based speed estimation. Since a fall involves a unique pattern of speed transition and lasts a certain duration, DeFall uses the time series of speed/acceleration captured continuously

Y. Hu, F. Zhang, C. Wu, B. Wang, and K. J. R. Liu are with the Department of Electrical and Computer Engineering, University of Maryland, College Park, MD, 20742, and the Origin Wireless Inc., Greenbelt, MD, 20770

E-mail: {yhu1109, fzhang15, cswu, bebewang, kjrliu}@umd.edu.

instead of the instantaneous values for identifying fall events. This can tremendously reduce the unwanted false alarm in a real environment. However, as we deal with time series, the temporal variability in time series brings up another challenge. To adapt to the non-linear compression or stretching over time, we apply the augmented dynamic time warping (DTW) based algorithms for the time series processing.

DeFall consists of two key components: the offline *template-generating stage* and the online *decision-making stage*. In the offline stage, a representative template for speed and acceleration series is generated. After that, the similarity between real-time speed/acceleration series and the template is evaluated in the online stage to detect a fall.

Since the speed and acceleration are inherent properties of the human motion that are independent of the static background environment, DeFall needs only one-time light training and is robust against different environments in an unsupervised manner. Also, thanks to the rich-scattering model used in speed estimation, the system can work very well under both line-of-sight (LOS) and NLOS scenarios.

To evaluate the performance of DeFall, extensive experiments have been conducted in a typical indoor environment in various settings. We first use a human-like dummy with a similar size and weight to a real human to carry out more than 800 fall experiments under LOS and NLOS to verify the feasibility and calculate the detection rate (DR). We also test the false alarm rate (FAR) while the real human performs daily indoor activities including walking and sitting. Furthermore, more real human fall samples are applied to validate the effectiveness of the proposed system. The experimental results show that DeFall can achieve a DR larger than 95% on real falls with an FAR of 1.47%, outperforming existing solutions in terms of both accuracy and robustness. The contributions of this work are summarized as follows:

- To the best of our knowledge, the proposed system is the first device-free fall detector that leverages the accurate time series of speed and acceleration estimated from WiFi channel state information (CSI).
- The proposed system works well in both LOS and NLOS scenarios, getting rid of the limitation of coverage while also protecting privacy.
- Through long-term testing, the system is verified to be robust against other daily activities as well as the falling of objects while keeping a high detection rate on real falls.
- Based on the performance comparison with other existing methods, our system can work independently without any re-training in a changing environment.

The rest of the paper is organized as follows. Section II reviews related works. Section III presents the basic principles of DeFall. Section IV depicts the system design and implementation. The performance of the proposed system is studied and evaluated in Section V and Section VI. Lastly, concluding remarks are given in Section VII.

II. Related Work

Thanks to the rapid development of Internet of Things (IoT) technologies and wireless sensing research, there are plenty of wireless IoT applications emerging, including fall detection systems. In this section, we review the literature on indoor activity recognition, with particular interests in fall detection. Existing works on passive wireless sensing can be categorized into different groups based on the features extracted from the wireless channel as Table I shows: radar-based, RSSI-based and CSI-based systems.

Radar-based systems detect events relying on specialized devices that are not readily available in homes. Many of them infer the motion of the reflector by evaluating the Doppler frequency shift and extract micro-Doppler signatures for recognizing finer body movements, such as activity monitoring [25], [26], gesture recognition [37], and fall detectors [16], [17]. Millimeter-wave (mmWave) radars, operating at higher transmit frequencies than commercial WiFi, provide better velocity resolution and capture more details on motion of different body parts [27], [38], [39]. Also, Ultra-wideband (UWB) radar, which has a high resolution due to the wide bandwidth, has also been proposed to classify indoor activities and detect falls [18], [19]. [18] proposes a time of arrival (TOA)-based feature extraction approach based on the received UWB signals. [19] approaches UWB-radar-based fall detection by applying a convolutional long short term memory (ConvLSTM) structure. [40] combines CNN and state machine and adopts a large-scale dataset to detect falls in various environments. However, although radars may have higher ranges or frequency resolutions, they usually require LOS for reliable operation. Therefore they can only detect falls in a very limited coverage and are also limited by the requirement of extra specialized dedicated devices. Further, the speed estimation derived from Doppler shift by radars varies for different moving directions and the heading direction of the subject is usually predefined [41].

Some other works on activity recognition and fall detection use commodity devices. Commercial wireless devices, such as WiFi infrastructures, are available in most indoor spaces and allow more flexible low-cost deployment. Chetty et al. apply passive WiFi radar (PWR) to realize the through-the-wall human sensing [35] and overcome the coverage limitation of traditional radars. However, PWR, which also relies on the principle of radars, collects Doppler information and therefore is also direction/location dependent and requires directional antennas [36].

Another widely-used method is using the received signal strength indicator (RSSI) to characterize indoor activities, either on WiFi or other wireless devices. For example, [28] explores WiFi ambient signals for RSSI fingerprints of different activities. However, since RSSI measures the overall amplitude response of multiple superposed subcarriers, it loses the phase information as well as the detailed information of each frequency component. Therefore it suffers from dramatic performance degradation in complex situations due to multi-path fading and temporal dynamics [42], limiting its stability and reliability in practical applications.

CSI, which measures both amplitude and phase information on different frequency components, provides finer-grained information for a propagation environment and becomes popular in the field of wireless sensing recently. Different from the

Methodology	Existing works	Limitations
Radar-based	Indoor activity recognition [25]–[27] Fall detection [16]–[19]	Limited detection range Cannot be integrated with commercial WiFi Specialized device required Doppler signature affected by moving direction
RSSI-based	Indoor activity recognition [28], [29] Fall detection [30]	Coarse granularity High sensitivity to environmental changes Multiple devices required
CSI-based	Indoor activity recognition [31]–[33] Fall detection [20]–[23]	Re-training required in new environments Performance degrades with LOS path blocked
PWR	Indoor activity recognition [34] Human sensing [35], [36]	Extra peripherals and directional antennas required Doppler signature affected by moving direction Stable reference channel required

TABLE I: Summary on related works.

Reference	Features	Claimed DR	Claimed FAR	Environment-independent
WiFall [20]	Variance	87%	18%	✗
RT-Fall [21]	Phase difference	91%	11%	✗
FallDeFi [22]	Spectrogram	94.33%	14.92%	✗
TL-Fall [23]	Frequency	86.83%	15.29%	✗
DeFall	Speed	95.80%	1.47%	✓

TABLE II: A brief summary of different CSI-based approaches to fall detection and the claimed performance.

mechanism of PWR, CSI is the standard information that can be extracted from commodity WiFi devices. By analyzing CSI accessible on mainstream devices nowadays, one could monitor indoor activities and detect indoor events, such as Wi-chase [31], CRAM [32] and TRIEDS [33]. In [20], Wang and Han et al. design WiFall, a WiFi-based unobtrusive fall detection system that extracts features from the CSI amplitude information to detect falls, while RT-Fall [21] exploits the efficacy of phase difference for activity segmentation and fall detection. FallDeFi [22] uses conventional short-time Fourier transform (STFT) to extract time-frequency features to sense the environmental changes and detect falls. Sensing-Fi [43] detects falls based on WiFi signals together with ground-mounted accelerometer measurements to capture floor vibrations. Unfortunately, as illustrated in Table. II, since the features extracted in the existing WiFi-based fall detection systems above are environment-dependent, the trained classifiers in these works suffer from the impact of environmental changes and cannot be generalized well to new environments without performance degradation. Re-training is required in these systems when the environmental settings change, which makes them impractical as it is not suitable to ask users to fall and collect training data every time the placements of furniture or the deployments of the devices get changed. TL-Fall [23] applies transfer learning to mitigate environmental influence and reduce the training workload, while light re-training is still needed in new environments and consecutive activities cannot be handled as activity segmentation is required before signal processing. In addition, an earlier version of this work has been published in [44] with a fixed sampling rate which may not be energy-efficient as the proposed fall down detection system requires a high sampling rate.

To address these challenges, in this work we propose DeFall that explores the inherent features of a fall and works well with only light training overhead and adaptive sampling rate based on a novel motion detector that is independent of the environment and can be put into use once deployed in any new environment without any re-training or calibration.

III. Preliminaries

In this section, the distinct speed pattern of a fall event is first presented. Then the definition of physical layer CSI is reviewed, and further, the principles of CSI-based motion detection and speed estimation are illustrated.

A. Distinct Characteristics of Fall Events

Different types of falls might happen in our daily life. Some are assisted falls occurring where the subject is assisted by another person or other supporting objects during the falling process. Unassisted falls occur unexpectedly without any support due to extrinsic environmental factors such as spills on the floor or intrinsic risk factors such as impaired gait. Compared to assisted falls, unassisted falls are closer to free falls and have larger speeds at the moment of hitting the ground, leading to a higher risk of causing severe injuries or even death [45]. Therefore the system we propose focuses mainly on detecting unassisted falls and especially those when the subjects fall from a standing position which produces the largest speed.

Speed and acceleration are two characteristics that are usually used to describe motion. Intuitively, fall can be viewed

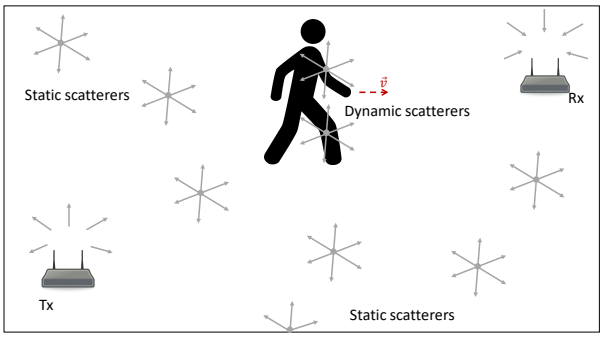

Fig. 1: Indoor rich-scattering model.

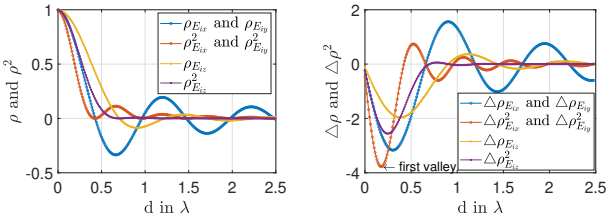

(a) Theoretical spatial ACFs.

(b) Theoretical differential of spatial ACFs.

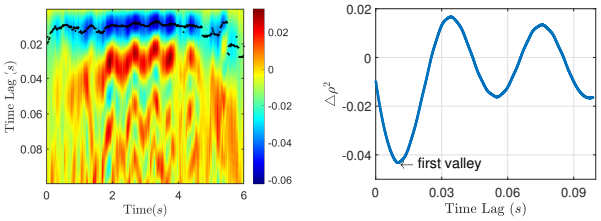

(c) Differential ACF of response power and the valley location.

(d) Instance of differential spatial ACF of response power.

Fig. 2: Spatial ACF and its differential for EM wave components.

as a type of abnormal indoor event with abnormal speed and acceleration and therefore they are both considered as the unique characteristics that help distinguish falls from other daily activities. The uniqueness resides not only in the absolute values of speed and acceleration during a fall but also in how they change over time. More specifically, as a human falls to the ground, his/her body will experience a rapid acceleration first. Once the body hits the floor, the body speed reduces to nearly zero sharply. In fact, most of the unexpected falls exhibit a similar pattern and this implies the feasibility of developing an environment-independent system by monitoring the speed and acceleration variation, which is the foundation of DeFall.

B. Speed Estimation from WiFi CSI

In wireless communication, CSI, which also refers to channel frequency response (CFR), describes the propagation of the signals from the transmitter (Tx) to the receiver (Rx). The estimate of the CSI over a subcarrier with frequency f at time t can be represented as

$$H(t,f) = \frac{Y(t,f)}{X(t,f)}, \tag{1}$$

where $X(t,f)$ and $Y(t,f)$ are transmitted and received signals. The transmitted WiFi signals experience multiple reflections in their propagation in indoor environments, and therefore CSI contains a lot of useful information on the channel conditions, which implies that we could capture the changes of the surrounding environment through CSI.

Since the unique pattern of the series of speed is utilized, it is critical to have an accurate and reliable estimate of the speed based on WiFi CSI, which is not trivial due to the multi-path effects of the indoor propagation. Some device-free CSI-based speed estimators [46]–[48] have been proposed and most of them make use of the Doppler frequency shift (DFS) to calculate the speed of the human body, which have several limitations. First, DFS-based methods utilize the reflection model, assuming that the human body is simplified as a single reflector and produces only one dominant reflection path, which usually does not hold in a practical indoor environment with rich multi-path propagation. Second, to make sure the direct reflection path from human body has strong enough energy to be perceived, the existing works are limited to the LOS coverage since the moving body should be able to be "seen" by both Tx and Rx. Third, as indicated by [46], DFS induced by human motion is not only related to the motion speed but also depends on the relative location and direction with respect to the link. In addition, DFS-based speed estimators take CSI phase into account, while the phase of CSI on commercial WiFi devices cannot be measured accurately due to the phase synchronization errors between the WiFi Tx and Rx [49].

Inspired by WiSpeed [24], in this work we assume a practical rich-scattering environment, as shown in Fig. 1, and estimate the speed based on a statistical model of EM wave theory, which only makes use of the CSI magnitude information.

Specifically, the CSI magnitude can be measured through CSI power response $G(t,f)$ defined as

$$G(t,f) \triangleq \mid H(t,f) \mid^2 = \xi(t,f) + \epsilon(t,f), \tag{2}$$

where $\xi(t,f) = \|\vec{E}_{Rx}(t,f)\|^2$, and $\vec{E}_{Rx}(t,f)$ denotes the propagated signals. $\epsilon(t,f)$ denotes the additive noise, and $\xi(t,f)$ and $\epsilon(t,f)$ are assumed to be independent of each other.

It has been shown in [24] that the speed of a moving object can be reliably estimated by evaluating the autocorrelation function (ACF) of $G(t,f)$. The theoretical ACF of $G(t,f)$, $\rho_G(\tau,f)$, can be derived as

$$\rho_G(\tau,f) = \frac{\sigma_\xi^2(f)}{\sigma_\xi^2(f)+\sigma_\epsilon^2(f)}\rho_\xi(\tau,f) + \frac{\sigma_\epsilon^2(f)}{\sigma_\xi^2(f)+\sigma_\epsilon^2(f)}\delta(\tau), \tag{3}$$

where τ is the time lag of the ACF. $\sigma_\xi^2(f)$ and $\sigma_\epsilon^2(f)$ are the variances of $\xi(t,f)$ and $\epsilon(t,f)$, respectively. $\rho_\xi(\tau,f)$ and Dirac delta function $\delta(\tau)$ are the ACFs of $\xi(t,f)$ and $\epsilon(t,f)$. When $\tau \neq 0$, we have $\delta(\tau) = 0$ and $\rho_G(\tau,f)$ can be further

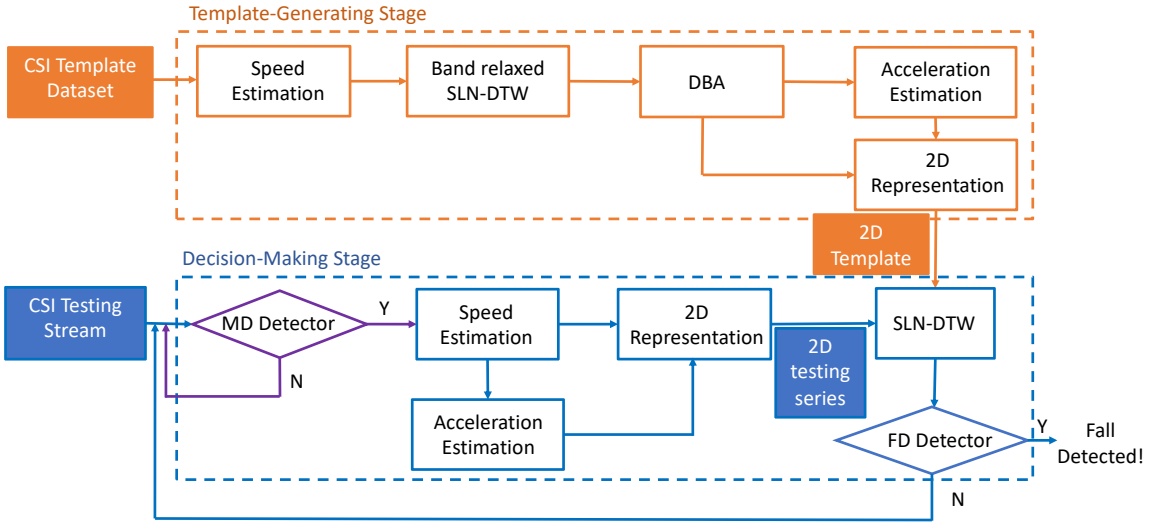

Fig. 3: An overview of DeFall.

derived based on the statistical theory of EM waves [50] as

$$\rho_G(\tau, f) = \sum_{u\in\{x,y,z\}} (C_1(f)\rho_{E_u}(\tau, f) + C_2(f)\rho^2_{E_u}(\tau, f)), \tag{4}$$

where $C_1(f)$ and $C_2(f)$ are scaling factors determined by the power reflected by all scatterers. $\rho_{E_u}(\tau, f)$ is the ACF of $\vec{E}_{Rx}(t, f)$ in u-axis direction where $u \in \{x, y, z\}$.

For the i-th dynamic scatterer that moves at speed v_i along z-axis, the scattered signal is denoted as $\vec{E}_{iu}(t, f)$. Then the components of its ACF $\rho_{E_{iu}}(\tau, f)$ in $\{x, y, z\}$-axes can be expressed as the following closed-form equations, respectively:

$$\begin{aligned}\rho_{E_{ix}}(\tau, f) &= \rho_{E_{iy}}(\tau, f) \\ &= \frac{3}{2}\frac{\sin(kv_i\tau)}{kv_i\tau}\big(1 - \frac{1}{(kv_i\tau)^2}\big) + \frac{3}{2}\frac{\cos(kv_i\tau)}{(kv_i\tau)^2},\end{aligned} \tag{5}$$

$$\rho_{E_{iz}}(\tau, f) = \frac{3}{(kv_i\tau)^2}\big(\frac{\sin(kv_i\tau)}{kv_i\tau} - \cos(kv_i\tau)\big), \tag{6}$$

where k denotes the wave number. Intuitively, the equations above have established a relationship between the ACF $\rho_G(\tau, f)$ and the presence of motion and also the moving speed.

- **The relationship between $\rho_G(\tau, f)$ and the presence of motion** From Eqn. (3), if motion is present in the propagation environment of WiFi signals, as $\tau \to 0$ we have $\delta(\tau) = 0$ and $\rho_\xi(\tau, f) \to 1$ due to the property of white noise and the continuity of motion [51]. Consequently, $\rho_G(\tau, f) \to \frac{\sigma^2_\xi(f)}{\sigma^2_\xi(f)+\sigma^2_\epsilon(f)} > 0$ as $\tau \to 0$. If there is no motion, the environment is static and the variance $\sigma^2_\xi(\tau, f) = 0$ and thus $\rho_G(\tau, f) = 0$ as $\tau \to 0$. Therefore the value of $\lim_{\tau\to 0}\rho_G(\tau, f)$ can indicate the presence of motion in the surrounding environment.
- **The relationship between $\rho_G(\tau, f)$ and the moving speed** For the simple case of all dynamic scatterers moving in the same speed and direction, without loss of generality we can assume the moving direction is in the z-axis and get the $\rho_G(\tau, f)$ as Eqn. (4) with its components expressed in Eqn. (5) and (6). Each component and its differential can be visualized in Fig. 2a and Fig. 2b, respectively. Observing that the first local valley of $\triangle\rho^2_{E_u}(\tau, f)$, $\forall u \in \{x, y\}$, happens to be the first local valley of $\triangle\rho_G(\tau)$ as well, we can extract the speed information of the moving scatterers by locating the first local valley of $\triangle\rho_G(\tau, f)$. Fig. 2c shows an example of $\triangle\rho_G(\tau)$ over time for a "walking" event, in which the the first valley locations are marked by the black dots. Fig. 2d shows a snapshot of the $\triangle\rho_G(\tau)$ in Fig. 2c.

In the case where a single subject, e.g., a human, moves within the coverage of the pair of Rx and Tx, the dynamic signals are dominated by the parts that are reflected by the human torso. Therefore it is reasonable to assume that in this case, all dynamic scatterers are moving at the same speed as well as in the same direction, and we can estimate the speed of the human using the proposed method to further detect a fall.

IV. DeFall Design

In this section, we depict the major modules in the DeFall system in detail. The system mainly consists of two stages as illustrated in Fig. 3. In the offline stage, the speed of a fall is estimated from the WiFi CSI by applying a statistical model on the radio propagation in an indoor rich-scattering environment. After that, DTW-based algorithms are performed to generate a representative template for a typical human fall. Then a fall event is detected in the online stage by evaluating the similarity between the patterns of real-time speed/acceleration estimates and the representative template. In addition, an online motion detection module is added before the fall detection module as a pre-judgment procedure.

A. Template-Generating Stage

In the offline template-generating stage, M CSI sequences of fall events are picked randomly and a "template database"

$\mathbb{S} = \{S_1, S_2, ..., S_M\}$ is built based on the corresponding estimated speed series.

1) Challenges in building a general template: To construct a single representative template, we perform an "average" on the database. Since the collected data are all time sequences, the result by direct point-to-point matching and averaging will be easily affected by sequence shift and misalignment. Therefore, the operation of distance measurement, as well as series alignment, will be performed in the DTW space [52].

However, there may exist redundant speed segments of other activities before or after the fall event, and the classic DTW algorithm is sensitive to the endpoints of the sequences. Therefore, the endpoints of the series should be carefully defined and the template database cleaning is required.

2) Template database cleaning: To remove the redundancy while adapting to the possible variability in event instances, we resort to the band-relaxed segmental locally normalized DTW (SLN-DTW) [53].

The basic idea of SLN-DTW is to detect low-distortion local alignments between the objective series S_x and a series S_y from the rest sequences $\{S_1, S_2, ..., S_{x-1}, S_{x+1}, ..., S_M\}$ by dynamic programming [53]. The original SLN-DTW aims at matching objective series S_x in the testing stream S_y with the assumption that S_x coincides exactly with the target event, which is not suitable since any of the collected series in $\mathbb{S}$ may contain redundancy. Therefore band-relaxed SLN-DTW in [53] is applied. It relaxes the boundary constraints of SLN-DTW so that the starting and ending points of S_x can be aligned adaptively and the common parts can be retrieved reliably.

To be specific, let i and j represent the indices of the objective sequence S_x and the testing sequence S_y, respectively. We can construct a grid $[1, \ldots, i, \ldots, L_1] \times [1, \ldots, j, \ldots, L_2]$, where L_1 and L_2 denote the lengths of S_x and S_y. With relaxed boundaries, the starting point of the optimal warping path is allowed to be located in the starting band $\{(i,j)|i \in [1, B_s]\}$ while the ending point is selected in the ending band $\{(i,j)|i \in [B_e, L_1])$. Then the accumulative distance matrix D and the length matrix L can be generated, where the elements of the two matrices, $D(i,j)$ and $L(i,j)$, represent the total cumulative distance and path length from a starting point $(i_s,\ j_s)$ to (i,j). And the cost function is defined as the ratio $C(i,j) = \frac{D(i,j)}{L(i,j)}$. The procedure of the band-relaxed SLN-DTW applied for template database cleaning can be summarized as:

Step 1 Initializing distance matrix D and length matrix L: For $\forall(i,j)$ where $1 \le i \le B_s,\ 1 \le j \le L_2$, we have

$$\begin{cases} D(i,j) = d(i,j) \\ L(i,j) = 1, \end{cases} \tag{7}$$

where $d(i,j)$ is the Euclidean distance between the i-th point in S_x and the j-th point in S_y.

Step 2 Iteration:

For $\forall(i,j)$ where $1 \le i \le B_s$ and $1 \le j \le L_2$, minimize $C(i,j) = \min_{(u,v)} \frac{d(i,j)+D(u,v)}{L(u,v)+1}$ where $(u,v) \in \{(i,j), (i-1,j), (i,j-1), (i-1,j-1)\}$. For each iteration, the updates of the corresponding D and L are

$$D(i,j) = \begin{cases} d(i,j), \text{ if } (u,v) = (i,j) \\ D(u,v) + d(i,j), \text{ otherwise,} \end{cases} \tag{8}$$

$$L(i,j) = \begin{cases} 1, \text{ if } (u,v) = (i,j) \\ L(u,v) + 1, \text{ otherwise.} \end{cases} \tag{9}$$

For $\forall(i,j)$ where $B_s < i \le L_1$, minimize $C(i,j) = \min_{(u,v)} \frac{d(i,j)+D(u,v)}{L(u,v)+1}$ where $(u,v) \in \{(i-1,j), (i,j-1), (i-1,j-1)\}$. For each iteration, update the corresponding D and L as

$$\begin{cases} D(i,j) = D(u,v) + d(i,j) \\ L(i,j) = L(u,v) + 1 \end{cases}. \tag{10}$$

Step 3 Trace back:

Find the minimum $C(k,j)$ for $k \in [B_e, L_1]$ and trace back along path (i,j) until $i = B_s$ to extract the optimum path across the central band $\{(i,j)|i \in [B_s, B_e]\}$. After that, if the cost to the next point is smaller than the current cost, i.e., $C(i_{next}, j_{next}) < C(i_{now}, j_{now})$, continue tracing back. Otherwise, stop and produce the optimum path.

Band-relaxed SLN-DTW is applied between every two speed sequences to extract their common parts. Therefore, for each objective series $S_x \in \{S_1, S_2, ..., S_M\}$, there are M-1 possible truncations with M-1 start indices $P_{x,s}$ and M-1 end indices $P_{x,e}$. And the part of S_x with indices lying in $[med(P_{x,s}), med(P_{x,e})]$ is regarded as the sanitized speed sequence of the fall event in sample S_x, where $med(P_{x,s})$ and $med(P_{x,e})$ are medians of the start indices and end indices, respectively. In this way, the template database is refined to $\hat{\mathbb{S}} = \{\hat{S}_1, \hat{S}_2, \ldots, \hat{S}_M\}$. Fig. 4a illustrates an instance of the sanitized speed series by applying SLN-DTW.

3) Averaging in the DTW measure space: The M cleaned speed series in the refined database $\hat{\mathbb{S}}$ are then scaled to the same length and averaged in the DTW measure space to construct a single representative profile. The problem to find an optimal average can be formulated as an optimization problem that given a set of template time series $\hat{\mathbb{S}} = \{\hat{S}_1, \hat{S}_2, ..., \hat{S}_M\}$, the averaged series $\bar{S}$ is the series that minimizes the sum of squared DTW distances between $\bar{S}$ and all of sequences in $\hat{\mathbb{S}}$

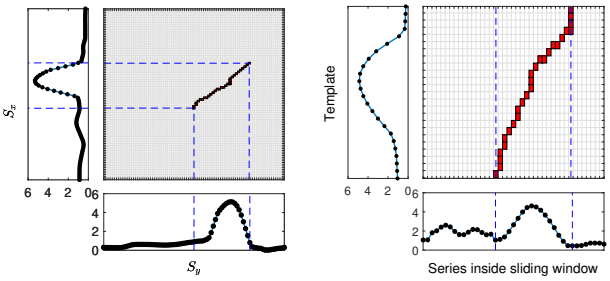

(a) Result of band-relaxed SLN-DTW to extract template.

(b) Result of a real-time detection by SLN-DTW.

Fig. 4: Applying the principle of SLN-DTW in series sanitization and fall detection.

as

$$\bar{S} = \arg\min_{S} \sum_{x=1}^{M} DTW^2(S, S_x). \tag{11}$$

The DTW distance of two sequences $DTW(A, B)$ is defined as the Euclidean distance between series A and series B along the optimal warping path as follows:

$$DTW(A, B) = \sqrt{\sum_{p^*=1}^{|P^*|} \|A[a_{p^*}] - B[b_{p^*}]\|^2}, \tag{12}$$

where P^* is the optimal warping path that minimizes the normalized distance as

$$P^* = \min_{P} \frac{1}{|P|} \sum_{p=1}^{|P|} \|A[a_p] - B[b_p]\|^2, \tag{13}$$

where a_p and b_p are indices of A and B associated with the p-th point on path P.

To solve the minimization problem (11) and get the optimal average series, DTW barycenter averaging (DBA) algorithm [54] is implemented. DBA is an iterative algorithm that refines an average sequence $\bar{S}$ on each iteration following an expectation-maximization scheme, whose convergence has been proved in [55]. The optimal speed time series $\bar{S}$, produced by DBA, is then considered as the speed template.

Besides speed, acceleration depicts the motion during a fall from another different point of view. To get a more comprehensive description of the fall events, we derive an acceleration series $\bar{S}'$ from the speed template $\bar{S}$ and combine them by point-to-point stitching to generate a 2-D template $\bar{S}_{2D}$. The efficacy of utilizing the 2-D combined template $\bar{S}_{2D}$ rather than a single 1-D template $\bar{S}$ or $\bar{S}'$ will be discussed in Section VI.

B. Decision-making Stage

As mentioned in Section III-A, fall events experience distinct speed and acceleration patterns which could be used for distinguishing falls from other indoor daily activities. However, a high sampling rate is needed for speed estimation [24]. To save energy and computation cost, in the decision-making stage, a low-rate motion detection (MD) module is included in addition to the fall detection (FD) module.

1) Motion Detection Module: As indicated in Section III-B, $\lim_{\tau \to 0} \rho_G(\tau, f)$ could be utilized as a criterion for MD. In practice, due to the limitation of the sampling rate, we could only use $\rho_G(\tau = \frac{1}{F_s}, f)$ to approximate $\tau \to 0$.

For the purpose of efficient energy-saving, the MD module with a low sampling rate is added as a pre-detection of human motion prior to the FD module, and the FD module is triggered only in the presence of motion.

2) Fall Detection Module: In the FD module, we apply a sliding window $\mathcal{W}$ on the incoming CSI stream. The testing speed sequence T is estimated from the CSI series in window $\mathcal{W}$. The acceleration sequence T' is further derived from T, followed by a combination operation to form a 2-D pattern T_{2D}.

Then fall events can be detected by comparing the testing time series T_{2D} with the template $\bar{S}_{2D}$. The corresponding similarity of the two series is evaluated in DTW space to adapt to misalignment of the two sequences in the time domain.

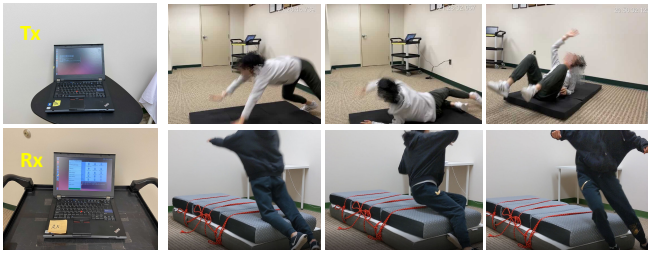

(a) Devices. (b) Fall examples.

Fig. 5: Illustrations for (a) devices for data collection and (b) examples for real falls including forward, lateral and backward falls.

Since the fall events involving different people may experience different duration, the series segmented by a length-fixed sliding window may also include other activities before or after the target event, which cannot be handled by the traditional DTW, and thus we adopt the SLN-DTW [53] again to localize the start and end instances of an event, as Fig. 4b illustrates. Regarding the template $\bar{S}_{2D}$ as the objective series and T_{2D} as the testing series, we set the lengths of starting and ending bands of $\bar{S}_{2D}$ to be 1 since the template $\bar{S}_{2D}$ is already sanitized.

By implementing SLN-DTW, the similarity of the testing stream T_{2D} and $\bar{S}_{2D}$ is evaluated. When the DTW distance between the testing series and the reference template is less than a preset empirical threshold γ, the testing sequence T_{2D} has a similar pattern to the reference fall template $\bar{S}_{2D}$ and the detector will alert that a fall occurs, where γ is empirically decided by experiments as well as the requirement of FAR and DR.

In the real-time monitoring, MD module keeps running with a lower sampling rate and as long as the motion is detected, the FD module starts working with a high sampling rate to estimate the speed and detect fall events. When the similarity between T_{2D} and $\bar{S}_{2D}$ stays low, i.e., the DTW distance larger than γ, for a long enough time, it switches back to MD module to save power consumption and computation cost.

V. Experimental Results

To build our DeFall system, we employ two laptops (Thinkpad T420) equipped with off-the-shelf WiFi network interface cards (Intel 5300) as the Tx and Rx, as shown in Fig. 5a. We use the Linux 802.11n CSI tool [56] to collect CSI measurements. Each of them is equipped with three omnidirectional antennas and the CSI stream over each pair of antennas has a total of 30 subcarriers. By default, the system works on WLAN channel 153 with a carrier frequency of 5.805 GHz and bandwidth of 40 MHz. In the MD module, the sampling rate is set to be 30 Hz. For FD module, to achieve a better speed estimation resolution to capture the high-speed motion, the Tx sends sounding frames with a channel sampling rate of 1500 Hz.

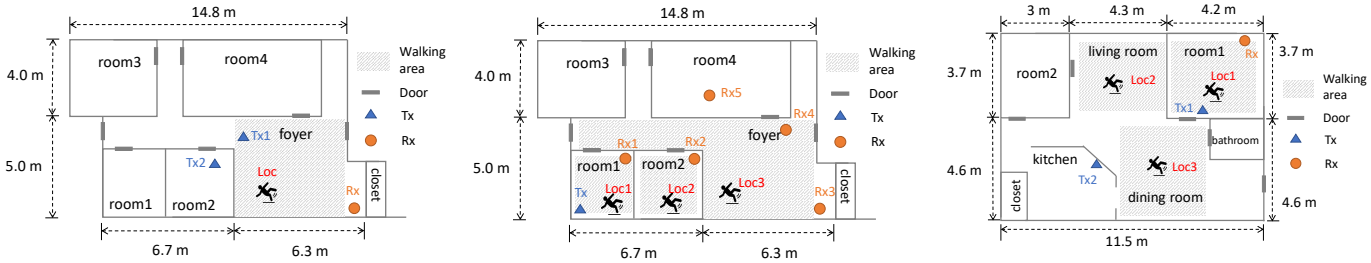

(a) Environment 1: typical office environment.

(b) Environment 2: different rooms and placements in the typical office.

(c) Environment 3: typical apartment environment.

Fig. 6: Experimental environments.

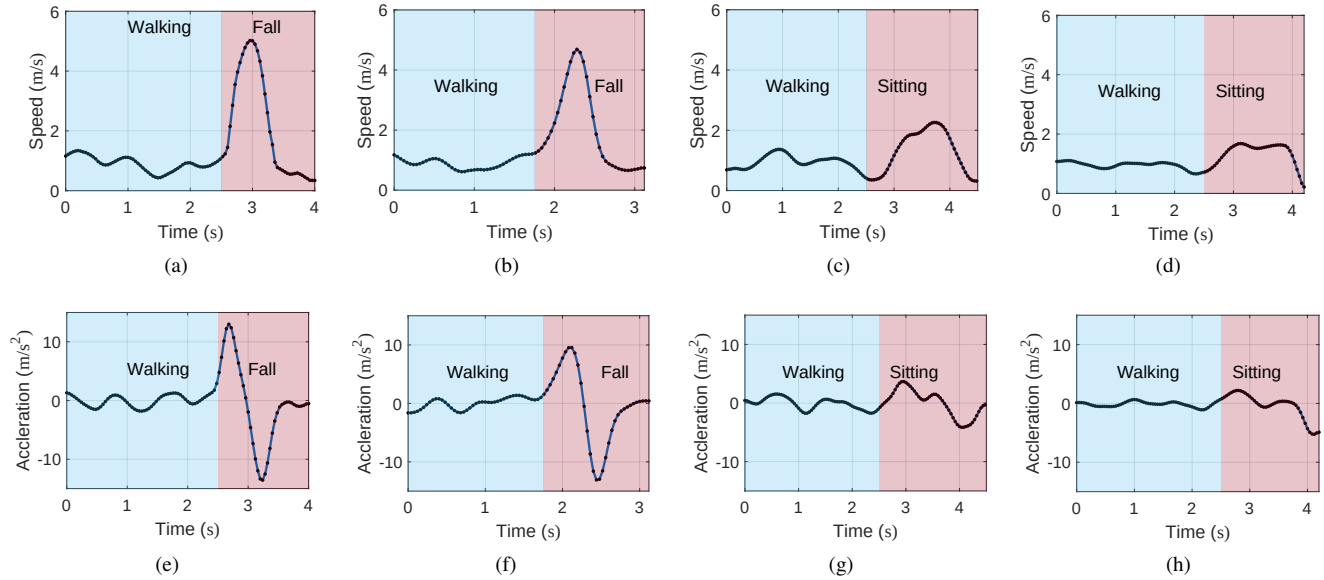

Fig. 7: Instances of speed and acceleration patterns for "walk-then-fall" and "walk-then-sit". (a)(e): Speed and acceleration for "walk-then-fall" under LOS; (b)(f): Speed and acceleration for "walk-then-fall" under NLOS; (c)(g): Speed and acceleration for "walk-then-sit" under LOS; (d)(h): Speed and acceleration for "walk-then-sit" under NLOS.

A. *Experimental Environments*

We evaluate DeFall with extensive experiments under various conditions (e.g., LOS and NLOS) at different locations in both office and home environments, with multiple volunteers involved. The detailed settings are shown in Fig. 6 with the locations of the Tx, the Rx, and the falling person marked. The data by a human-like dummy in environment 1 (Fig. 6a) is used for template-generating as well as detection algorithm verification. Then real fall/non-fall activities are performed by volunteers in all environments to further evaluate the impacts of environment diversity, user diversity and also types of falls. The ground truth is recorded by video.

In each environment, we change one of the Tx/Rx and conduct experiments with different placements under both the LOS and NLOS scenarios. Under the LOS scenario, Tx and Rx could both "see" the subject, while in the NLOS case, there does not exist any direct link between the subject and one or more devices, which is very common for an indoor environment. Specifically, in environment 1 (Fig. 6a) and environment 3 (Fig. 6c), the Tx is deployed on positions Tx_1/Tx_2 under LOS/NLOS conditions. In environment 2 (Fig. 6b), only Rx_1 is under the LOS scenario, while the other placements correspond to the NLOS cases.

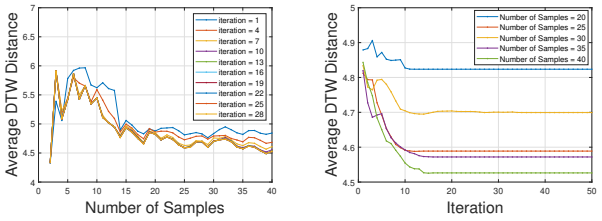

(a) Average DTW distance versus sample size in DBA algorithm.

(b) Average DTW distance versus number of iterations in DBA algorithm.

Fig. 8: Investigation of DBA factors.

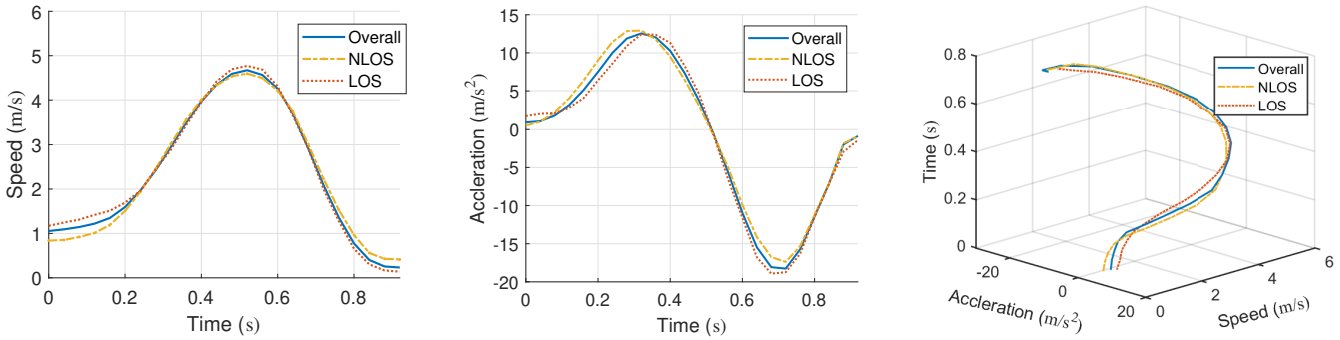

(a) Speed templates. (b) Acceleration templates. (c) 2D templates.

Fig. 9: Templates.

B. Data Collection

The data collection is carried out on different days lasting for more than three months, during which the surrounding propagation environment keeps changing, including the changes of the placements of furniture, the opening or closing of doors and windows, etc. To verify the feasibility of DeFall, we first use a human-like dummy to collect both the template data and testing data. After that, the samples from real human falls, as illustrated by Fig. 5b, are further studied to evaluate the effectiveness of the system.

In the verification experiments, we consider both separate fall events and continuous motion followed by falls. "Stand-then-fall", which represents falling from a stationary standing posture, is realized by first letting the dummy stand straight and then making it fall freely; while "walk-then-fall", indicating the falls happen after the continuous walking motion, requires the experimenter to walk around the standing dummy at a normal speed and then make it fall. Instances of the speed/acceleration patterns for "walk-then-fall" and "walk-then-sit" under both LOS and NLOS scenarios are presented in Fig. 7, where we can observe the distinct patterns between falls and other activities such as sitting and walking. After the long-term data collection, there are 846 fall samples from the dummy and 814 non-fall samples for verification in total as Table III illustrates.

In order to prove that our system can work well in real world, we further evaluate its performance based on real human falls. We first involve three volunteers (1 female, 2 males) for multiple long-term experiments to study the impact of environment diversity, the presence of ambient motion, and the types of falls (forward, backward and lateral falls). To investigate the impact of user heterogeneity, we involve 7 more volunteers at different ages to perform different falls.

C. Generated Templates

In the offline template-generating stage, we build the template dataset on the fall samples from the dummy. There are two factors to be selected in the DBA algorithm, i.e., the size of template database and the number of iterations. The investigation of these two factors can be seen in Fig. 8. In Fig. 8a, the average DTW distance gets more stable as the size of template database increases to 25, while in Fig. 8b it converges after around 15 iterations. Therefore the number of iterations and the size of the template database are reasonably set to be 20 and 40, respectively.

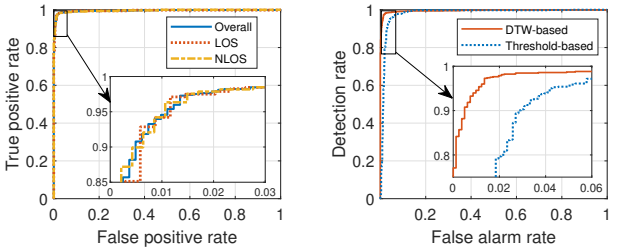

(a) ROC curves for overall, LOS and NLOS cases. (b) ROC curve of DeFall compared with threshold-based method in WiSpeed.

Fig. 10: ROC curves for (a) different scenarios and (b) comparison with the threshold-based method in WiSpeed.

The generated template after refinement and averaging is presented in Fig. 9. As we can observe, the template has the same tendency as expected. The speed rises to a peak value first and then drops, while the acceleration is positive first and then becomes negative. Also, it can be found that the templates of LOS and NLOS are highly consistent with each other. Since the speed estimation in DeFall is based on the rich-scattering model, as long as the target is within the coverage of the radios, the system can capture the speed accurately using either the LOS or NLOS link, preserving not only the average speed but also the precise speed changes. Due to the high consistency between the LOS and NLOS scenarios, we use both LOS and NLOS data for template-generating and apply the overall template in the detecting phase.

D. Performance Evaluation

1) Evaluation metrics: The evaluation metrics of the system performance are detection rate and false alarm rate. Detection rate, shorted as DR, is defined as the percentage

Scenario	Events		Number	DR/FAR (DeFall)		DR/FAR (WiFall)		DR/FAR (FallDeFi)	
LOS	Fall	Stand-then-Fall	424	97.40%	97.10%	75.71%	74.32%	91.04%	89.58%
		Walk-then-Fall	94	95.74%		68.09%		82.98%	
	non-Fall	Walking	167	0.00%	1.45%	16.77%	18.90%	10.18%	12.79%
		Sitting down	177	2.82%		22.03%		15.25%	
NLOS	Fall	Stand-then-Fall	270	98.15%	97.56%	70.37%	69.82%	85.19%	84.45%
		Walk-then-Fall	58	94.83%		67.24%		81.03%	
	non-Fall	Walking	212	0.47%	1.49%	15.09%	17.23%	8.96%	10.43%
		Sitting down	258	2.33%		18.99%		11.63%	
Overall	-			97.28%/1.47%		72.58%/17.45%		87.59%/11.43%	

TABLE III: Comparison results with WiFall and FallDeFi.

of correctly detected falls among all falls:

$$DR = \frac{\#\ of\ detected\ falls}{\#\ of\ total\ falls}, \tag{14}$$

while false alarm rate, simplified as FAR, is the percentage of non-falls that are mistaken as falls among all non-falls:

$$FAR = \frac{\#\ of\ wrongly\ detected\ nonfalls}{\#\ of\ total\ nonfalls}. \tag{15}$$

2) Receiver operating characteristic (ROC) curve: The threshold γ in the decision-making stage plays an important role in determining the boundary between fall and non-fall events, and therefore it has to be selected carefully. To evaluate the performance of DeFall, instead of proposing the specific threshold directly, we first calculate the DR and FAR with various thresholds and generate the overall ROC curve as illustrated by Fig. 10a. We also investigate the ROC curves in LOS and NLOS scenarios, respectively. As seen, there exists a trade-off between DR and FAR. If the γ is small, then there tends to be fewer speed sequences to reach the standard, i.e., the smaller γ is, the lower the DR is, while also getting a lower FAR. Note that the ROC curves of LOS and NLOS overlap with each other. Also, both of them are highly similar to the overall ROC trend, verifying the consistency of the proposed system in LOS/NLOS scenarios.

3) Effectiveness of the DTW-based pattern matching: In the previous work WiSpeed [24], a simple threshold-based method is applied to detect falls and two features are proposed: (i) the maximum speed; (ii) the maximum change in acceleration within 0.5 s. In DeFall, we use the same CSI-based speed estimator as Wispeed but improve the detection performance by adding the DTW-based pattern matching for making a decision. To show the effectiveness of the DTW-based detection module, we also get the ROC curve of WiSpeed by simultaneously adjusting the boundaries for the two aforementioned features and compare it with DeFall as shown in Fig. 10b. As Fig. 10b illustrates, at the same level of FAR, the DR of DeFall is higher than WiSpeed. The area under the curve (AUC) of the ROC of DeFall is larger as well, proving a better performance. In particular, when the FAR is less than 1.5%, DeFall can still achieve a high DR over 95% while the corresponding DR of WiSpeed drops to a level less than 75%.

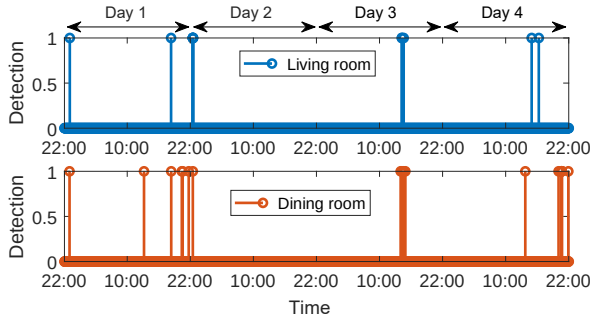

Fig. 11: Long-term testing in an apartment environment.

E. Robustness to Indoor Activities

For a fall detection system, DR is very crucial due to the high risk of miss detection. On the other hand, FAR is also essential since other daily activities are performed most of the time in practice. Thus a system that yields a low FAR while keeping a reasonable DR is preferred. In this work, the threshold yielding an overall FAR 1.47% is selected for further system evaluation and the corresponding overall DR is 97.28%.

The results of DR and FAR for all types of events are summarized in Table III. According to the results, DeFall succeeds in performing a high DR and low FAR under both LOS and NLOS scenarios. Comparing the results of different fall events, we can notice a higher DR on "stand-then-fall" events than "walk-then-fall" events since "walk-then-fall" may introduce interference to the speed estimation at the beginning of falls. Also, among the non-fall events, as "sitting-down" experiences an acceleration followed by a deceleration, which is more similar to the fall pattern than "walking", it is can be observed that FAR of "sitting-down" is slightly higher than that of "walking".

We implement WiFall [20] and FallDeFi [22] for the comparative study. WiFall extracts seven different features for classification based on the variation of CSI amplitude over time, while FallDeFi selects features from the STFT spectrogram and the power burst curve (PBC). To make a fair comparison, we optimize the parameters in these two works to adapt to our dataset. We apply 40 fall samples to generate the template in DeFall, while we use 80 samples (40 falls and 40

Objects	Material	Size/Weight	FAR
Bottle	Plastic, water	$0.5kg$	0.0%
Bag	Nylon	$1kg$	0.0%
Plate	Plastic	$Radius = 12cm$	0.0%
Plate	Metal	$Radius = 10cm$	0.0%
Book	Paper	$22cm \times 18cm$	0.0%
Box	Paper	$17cm \times 17cm$ $\times 25cm,\ 0.8kg$	0.0%
Chair	Wood	$50cm \times 40cm$ $\times 58cm,\ 3kg$	0.0%

TABLE IV: Impact of falling objects.

	Forward	Backward	Lateral	Average
User 1	96.67%	95.56%	94.44%	95.56%
User 2	94.44%	96.67%	93.33%	94.81%
User 3	95.56%	97.78%	97.78%	97.04%
Average	95.56%	96.67%	95.19%	95.80%

TABLE V: Detection rates on different fall types.

	Env. 1		Env. 2					Env. 3	
	LOS	NLOS	LOS	NLOS				LOS	NLOS
	Tx_1	Tx_2	Rx_1	Rx_2	Rx_3	Rx_4	Rx_5	Tx_1	Tx_2
Loc 1	97.78%	95.56%	100%	97.78%	91.11%	95.56%	93.33%	97.78%	95.56%
Loc 2	-	-	-	100%	93.33%	93.33%	91.11%	-	95.56%
Loc 3	-	-	-	-	97.78%	97.78%	93.33%	-	97.78%
Average	97.78%	95.56%	100%	98.89%	94.07%	95.56%	92.59%	97.78%	96.30%

TABLE VI: Detection rates in various environments.

non-falls) to train the classifiers in WiFall and FallDeFi. The results in Table III demonstrate that DeFall outperforms both WiFall and FallDeFi with a higher overall DR (24.7% higher than WiFall and 9.69% higher than FallDeFi) and a lower FAR (15.98% lower than WiFall and 9.96% lower than FallDeFi). In addition, under both LOS and NLOS scenarios, DeFall also performs better in terms of the corresponding DR and FAR. The reasons for this performance enhancement can be attributed to the environment-independent speed information extracted by DeFall and the DTW-based pattern matching which adapts to the consecutive activities. More specifically, the features extracted in WiFall are based on the signal variation and could be different in different settings, while the speed estimated in DeFall is an inherent property of falls. Although compared with WiFall, FallDeFi devises more robust features using time-frequency analysis, its spectral features are partly dependent on the signal strength and do not take the detailed change pattern of falls into consideration. We also observe that the performance of WiFall and FallDeFi degrades especially for consecutive events such as "walk-then-fall". This is because WiFall and FallDeFi either assume segmented activities or apply the "event duration" as a feature, which can easily lead to misclassifications if falls and other normal activities cannot be separated reliably, while DeFall employs a sliding window combined with the pattern matching approach which is more flexible to handle consecutive activities.

To take all possible daily activities into consideration and test the robustness of the system in practical, we further run the system in the same apartment (Fig. 6c) for four days. Specially, we deploy two pairs of transceivers to cover the main motion areas - living room and dining room, respectively. The participant stays in the apartment every day and may perform any daily activities in the monitored areas. No fall happens during the testing. We apply the same template and detection algorithm to the collected speed series. The experiment results for the long-term continuous test can be found in Fig. 11. The decision is output every second and the corresponding false alarms are counted. We have only 12 and 19 false alarms in total during the four-day testing in the living room and dining room. On average, we have 3 and 6.3 false alarms per day, which is acceptable considering the involved complicated daily activities.

F. Robustness to Falling Objects

There are fall-like events that may cause false alarms, such as falls of chairs and dropping a small object to the ground. To test the robustness of the system against the interference from these events, extensive fall experiments are conducted on objects with different sizes and different materials. For small objects, each of them is lifted up and then dropped from a height of 1m, which is repeated 50 times at various locations to evaluate a reliable FAR. We also repeat testing a falling wooden chair. The corresponding result listed in Table IV presents that all the FARs are 0.0%, verifying the robustness of DeFall. This is because common objects which can be lifted up are usually much smaller than a human body and therefore, even if dropped from a high position, they produce fewer dynamic scatterers and cause less disturbance to the environment. In such a case, the speed or acceleration values cannot be detected or the values are not continuous. For falling chairs, they always fall with lower centers of gravity and have smaller speeds than human falls.

G. Types of Falls

Three volunteers are involved in the experiments of real falls. In this subsection, we study the impact of the orientation of a fall, i.e., forward, backward and lateral. Each of the three volunteers performs 5 forward falls, 5 backward falls and 5 lateral falls in all settings. To better mimic real-world falls, the subjects first perform normal activities, either walking or standing still, and then fall in different directions under each setting. The overall results are summarized in Table. V. Taking the experiments in all environments into account, we find that the falls in all the considered directions can achieve a detection rate above 95.00%. The results are as expected because the proposed approach is independent of the moving/falling directions.

H. Environment Diversity

To validate the robustness of DeFall to diverse environments, extensive experiments are carried out in both office and home environments. Also, the locations of Tx and Rx are changed. During the experiments, each subject performs

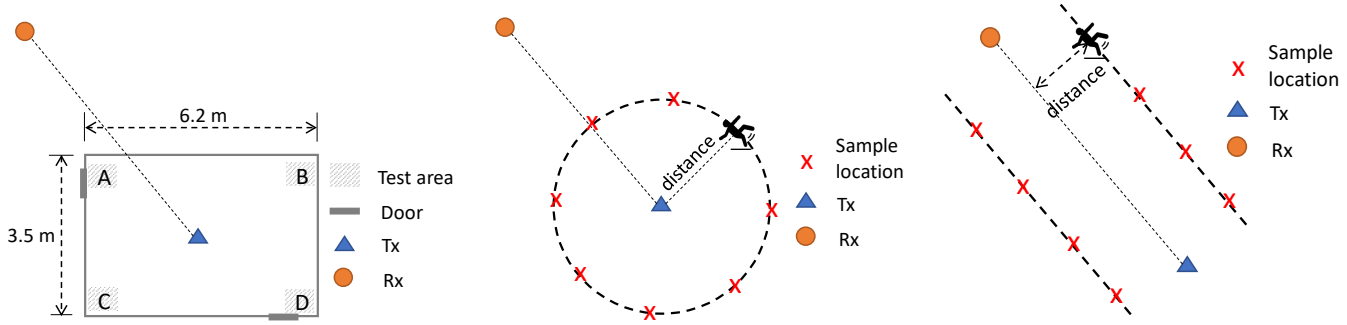

(a) Setting 1: NLOS scenario. (b) Setting 2: LOS scenario. (c) Setting 3: LOS scenario.

Fig. 12: Settings for analyzing coverage.

Training/Template	Testing	DR (DeFall)	DR (WiFall)	DR (FallDeFi)
Env. 1	Env. 1	96.67%	72.22%	90.00%
LOS in Env. 1	NLOS in Env. 1	95.56%	53.33%	82.22%
Env. 1	Env. 2	95.37%	56.11%	81.30%
Env. 1	Env. 3	96.67%	52.78%	76.11%

TABLE VII: Impact of environmental changes.

	User 1	User 2	User 3	User 4	User 5
DR	95.56%	94.81%	97.04%	91.67%	97.22%
weight (kg)	77	50	84	70	62
height (cm)	174	166	168	172	175
	User 6	User 7	User 8	User 9	User 10
DR	94.44%	97.22%	100%	94.44%	97.22%
weight (kg)	60	90	70	91	53
height (cm)	169	178	171	170	160

TABLE VIII: Detection rates of different users.

15 falls in different directions on different positions marked in the floorplan shown in Fig. 6. As reported in Table VI, a minimum detection rate of 91.11% can be achieved in different environments. The high detection rates are as expected because the proposed approach is environment-independent.

We also highlight such independence by comparing it with WiFall and FallDeFi. As Table VII indicates, when we classify the data collected in a different environment from the training dataset, DeFall outperforms both of WiFall and FallDeFi with a higher detection rate.

I. User Diversity

As different users have different heights, body shapes and gait styles, and a reliable fall detector should not be affected by the diversity of users, it is non-trivial to investigate the impact of the user heterogeneity on the performance. To do this, during a two-week experiment, 7 more volunteers with ages ranging from 23 to 59 are asked to perform falls at various locations in environment 2. Similar to the previous experimental procedure, the volunteers perform random activities before falling. Each volunteer falls three times (1 forward, 1 backward and 1 lateral) under each setting. Combining the experiments of different displacements and different locations, we focus on studying the impact of user diversity and summarize the results in Table VIII. For Users 1-3, we have 270 samples each, while for Users 4-10, 36 samples are collected by each user. The users have weights varying from 50 kg to 91 kg and heights varying from 160 cm to 178 cm. Among all the ten subjects, User 7 is the tallest and User 9 is the heaviest while both User 7 and User 9 experience miss detection. Therefore, although a greater height and weight indicate more dynamic scatterers on the torso for signal propagation, we cannot conclude that there is an obvious monotonic relationship between users' heights or weights and the detection performance based on the samples from ten subjects.

	w/ other moving person				w/o other motion
	light motion		heavy motion		
	3-5 m	$>$ 5m	3-5 m	$>$ 5m	
LOS	12/15	15/15	8/15	15/15	15/15
NLOS	13/15	15/15	6/15	14/15	15/15

TABLE IX: Detection results with ambient motion.

J. Impact of Ambient Motion

In this part, we investigate the robustness of the DeFall system when a second subject is moving in the vicinity of the first falling subject, with both LOS and NLOS cases considered. Intuitively, two factors may affect the performance, the distance between the two subjects ("distance") and the motion strength of the second subject. To study their impacts, we conduct experiments with a distance of 3-5 m and $>$5 m between the two subjects while for the motion strength, we consider heavy motion (walking) and light motion (reading and typing). Under each setting, 15 fall events occur with different fall orientations, and the results are presented as the ratio of the number of detected falls to a total of 15 falls in Table IX. As we can see, when the second person is walking, the detection rate degrades as the distance decreases due to the interference from the other person. Nevertheless, some falls can still be detected even when the walking person is close. This is because the system estimates speed by localizing the first valley as Fig. 2d shows, which always corresponds to the highest speed of the massive scatterers. Therefore, the

	DR	FAR
A	95.45%	1.28%
B	91.30%	1.33%
C	95.45%	2.56%
D	90.91%	0.0%

TABLE X: DR and FAR under setting 1.

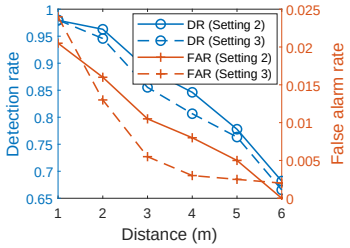

Fig. 13: DR and FAR under setting 2 and setting 3.

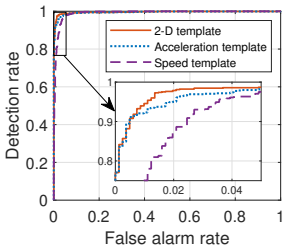

(a) ROC curves for 2-D template and 1-D separate templates.

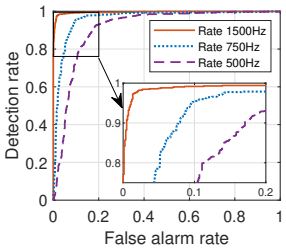

(b) ROC curves for different sampling rates.

Fig. 14: ROC curves for (a) comparison on 2-D template and 1-D separate templates and (b) different sampling rates.

high speed associated with a fall can still be captured. Also, the motion strength of the interfering person has a significant impact on the performance, and a light motion by the second person has much less interference than a strong motion.

In fact, fall detection mainly aims at protecting the elderly people who live alone by sending alarms to remote caregivers when the subject being monitored falls. If there is another person nearby, timely assistance is available and the harm to the subject experiencing a fall will be greatly reduced. Therefore, the slight degradation in the multi-user case has little impact on the applicability of DeFall as it ensures great performance for a single-user case and the cases when another user is relatively still or far away.

K. Coverage

It is important to provide a large coverage for a real-world fall detection system. For this purpose, we conduct experiments in a large empty hall to evaluate if falls that are far away from the devices can be detected. As shown in Fig. 12a, for the NLOS setting, the Tx is deployed at the center of a room with size $6.2\,\text{m} \times 3.5\,\text{m}$, the Rx is in the hall and 10 m away from the Tx, and falls are performed at four corners with the corresponding DR and FAR shown in Table X given the pre-selected threshold in Section V-E. For the LOS setting, in order to find the impact of the distance between the subject and devices, we first sample uniformly on positions marked with "X" along the circle centered around Tx with a changing radius as shown in Fig. 12b. In the second LOS setting shown in Fig. 12c, falls occur along lines parallel to the direct link. Massive fall samples are collected using the human-like dummy and a real human performs non-fall activities. Illustrated by Table X, the system under setting 1 can cover an area as large as a normal office. Also, revealed by Fig. 13, DR and FAR both decrease as the distance between the subject and devices increases.

VI. Discussion

In this section, we will discuss the result of applying 2-D template comparing with that of using only 1-D speed template and 1-D acceleration template, which demonstrates the necessity of combining the features into 2-D space. Also, we will study the impact of the sampling rate and investigate the speed distribution of activities. In addition, we evaluate the computation cost.

A. Necessity of 2-D Space

The 2-D combining step integrates the information contributed by speed and acceleration. The combination is based on different weights α and realized by $\bar{S}_{2D} = \left((1-\alpha)\bar{S}, \alpha\bar{S}'\right)$. By setting $\alpha = 0$, we can get the single speed template while the single acceleration template can be obtained through setting $\alpha = 1$. For 2-D space, we set α to be 0.5. The performance of the separate 1-D templates and combined 2-D template can be found in Fig. 14a. As shown, the 2-D combined template outperforms any single template as it provides a more comprehensive description of the events.

B. Impact of Sampling Rate

As described in Section IV, the sampling rate is a critical factor affecting the performance of our system. We now revisit the experimental results in Section V and evaluate the performance with different sampling rate F_s. The DR and FAR are studied under different sampling rates 1500 Hz, 750 Hz and 500 Hz, and their corresponding ROC curves are plotted in Fig. 14b. As illustrated, the overall trends for all the cases are the same, in which FAR increases as DR increases. However, the decrease of the sampling rate leads to a degradation in the performance of DeFall. This is because as the sampling rate gets reduced, the resolution of the ACF-based speed estimator degrades correspondingly, which will introduce more estimation errors and harm the detection accuracy.

C. Speed Distribution of Activities

Although the maximum speed of the template can be up to around $5\,m/s$, it does not mean the system can only detect falls with speeds reaching as high as $5\,m/s$. This is because the proposed template-based method not only depends on the single maximum speed value but also relies on the trend of speed, which relaxes the decision boundary compared with a hard-thresholding method.

To understand the system capability better, we divide our real fall/non-fall samples into different intervals $(0\ 1m/s]$, $(1m/s\ 2m/s]$, $\cdots$, $(5m/s\ 6m/s]$ based on their maximum speeds. The corresponding distribution is shown in Fig. 15a. Then we apply the same overall template and decision boundary and evaluate the corresponding DR/FAR in each individual

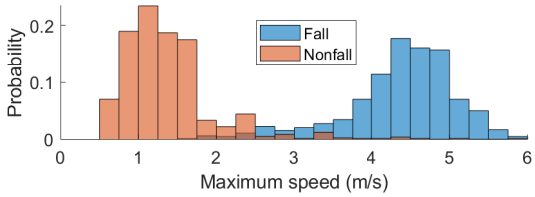

(a) Distribution based on the maximum speed.

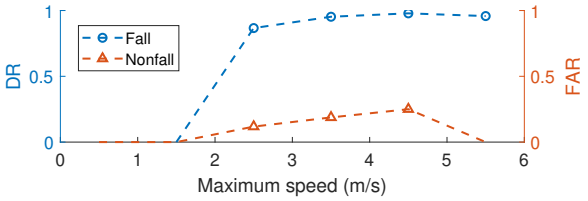

(b) DR/FAR in each maximum speed interval.

Fig. 15: Maximum speed distribution and DR/FAR for each maximum speed interval.

Stage	Module	CPU time (s)	CPU time (%)
Offline template generating (dataset size: 40)	Speed estimation	8.571322	96.23
	Database sanitization	0.168743	1.895
	DBA for average	0.165920	1.863
	2D representation	0.001251	0.014
	Total	8.9072	
Online computation for each output	Motion detection	0.000535	2.355
	Speed estimation	0.004661	20.52
	SLN-DTW & Detection	0.017519	77.13
	Total	0.0227	

TABLE XI: Processing time of DeFall.

interval, where the DR/FAR is the ratio of detection to the total falls/non-falls in that specific interval. As we can see, the maximum speeds of fall and non-fall series samples are distinct with a small overlapped part. The FAR and DR both increase with the speed, as illustrated by Fig. 15b. However, even if the falls and non-falls have the maximum speeds in the same interval, our system can still distinguish most of them with reasonable DR/FAR because of their distinct patterns over time.

D. Computation Cost and Realtime Realization

In the real-time scenario, as the extracted speed feature is independent of the environments, the offline stage can be completed ahead of time. Then the pre-trained template can be applied directly in the decision-making stage.

To evaluate the system computation effort, we repeat the process using MATLAB on a desktop with Intel Core i7-9700K processor and 32 GB memory. We record the average processing time. Table XI illustrates the CPU time for each module in the offline and online stages. Note that we do not require a massive amount of data for template generating, which significantly reduces the computation cost. The total pre-training process only takes an average CPU time of 8.9 s. In the online stage, to produce a decision output, it costs only 0.0227 s with a speed estimation module and a simple DTW-based similarity calculation, which is short enough for real-time applications.

E. Limitation

Since we only focus on the hard falls which may cause serious injuries, our approach only deals with unexpected falls such as stumbles or slips due to weak gait. Other types of falls such as falls slowly from a lower height, may result in a different speed pattern from what is described in this paper. To solve this problem, we need more analysis on the action decomposition to get a better understanding of the entire process of various falls. In this case, multiple templates and deep learning techniques may be required.

Another limitation is that since the algorithm can only estimate the approximate average speed of the moving objects in the environment, our system works well when there is a single person or no strong ambient motion close to the subject. However, this is fully compliant with the goal of our system to protect the elderly who live alone.

VII. Conclusion

In this paper, we propose DeFall, a novel environment-independent indoor fall detection system using commercial WiFi devices. The system extracts speed information to detect falls even through the walls with a single pair of transceivers. A real prototype is built to validate the feasibility and evaluate the performance in various environments. The results show that DeFall achieves a detection rate higher than 95% on real falls while maintaining a false alarm rate lower than 1.50% under both LOS and NLOS scenarios, without any scenario-tailored prior training.

References

[1] "Falls." [Online]. Available: https://www.who.int/news-room/fact-sheets/detail/falls. Accessed: April 2021.

[2] P. Melillo, R. Castaldo, G. Sannino, A. Orrico, G. de Pietro, and L. Pecchia, "Wearable technology and ecg processing for fall risk assessment, prevention and detection," in *2015 37th Annual International Conference of the IEEE Engineering in Medicine and Biology Society (EMBC)*, pp. 7740–7743, 2015.

[3] P. Pierleoni, A. Belli, L. Maurizi, L. Palma, L. Pernini, M. Paniccia, and S. Valenti, "A wearable fall detector for elderly people based on ahrs and barometric sensor," *IEEE Sensors Journal*, vol. 16, no. 17, pp. 6733–6744, 2016.

[4] J. Wang, Z. Zhang, B. Li, S. Lee, and R. S. Sherratt, "An enhanced fall detection system for elderly person monitoring using consumer home networks," *IEEE Transactions on Consumer Electronics*, vol. 60, no. 1, pp. 23–29, 2014.

[5] J. Dai, X. Bai, Z. Yang, Z. Shen, and D. Xuan, "Perfalld: A pervasive fall detection system using mobile phones," in *2010 8th IEEE International Conference on Pervasive Computing and Communications Workshops (PERCOM Workshops)*, pp. 292–297, IEEE, 2010.

[6] S. Abbate, M. Avvenuti, F. Bonatesta, G. Cola, P. Corsini, and A. Vecchio, "A smartphone-based fall detection system," *Pervasive and Mobile Computing*, vol. 8, no. 6, pp. 883–899, 2012.

[7] C.-C. Lin, P.-Y. Lin, P.-K. Lu, G.-Y. Hsieh, W.-L. Lee, and R.-G. Lee, "A healthcare integration system for disease assessment and safety monitoring of dementia patients," *IEEE Transactions on information Technology in Biomedicine*, vol. 12, no. 5, pp. 579–586, 2008.

[8] E. Auvinet, F. Multon, A. Saint-Arnaud, J. Rousseau, and J. Meunier, "Fall detection with multiple cameras: An occlusion-resistant method based on 3-d silhouette vertical distribution," *IEEE Transactions on Information Technology in Biomedicine*, vol. 15, no. 2, pp. 290–300, 2011.

[9] C. Rougier, J. Meunier, A. St-Arnaud, and J. Rousseau, "3d head tracking for fall detection using a single calibrated camera," *Image and Vision Computing*, vol. 31, no. 3, pp. 246–254, 2013.

[10] E. E. Stone and M. Skubic, "Fall detection in homes of older adults using the microsoft kinect," *IEEE Journal of Biomedical and Health Informatics*, vol. 19, no. 1, pp. 290–301, 2015.

[11] G. Mastorakis and D. Makris, "Fall detection system using kinect's infrared sensor," *Journal of Real-Time Image Processing*, vol. 9, no. 4, pp. 635–646, 2014.

[12] S. Gasparrini, E. Cippitelli, S. Spinsante, and E. Gambi, "A depth-based fall detection system using a kinect® sensor," *Sensors*, vol. 14, no. 2, pp. 2756–2775, 2014.

[13] X. Ma, H. Wang, B. Xue, M. Zhou, B. Ji, and Y. Li, "Depth-based human fall detection via shape features and improved extreme learning machine," *IEEE Journal of Biomedical and Health Informatics*, vol. 18, no. 6, pp. 1915–1922, 2014.

[14] B. Wang, Q. Xu, C. Chen, F. Zhang, and K. R. Liu, "The promise of radio analytics: A future paradigm of wireless positioning, tracking, and sensing," *IEEE Signal Processing Magazine*, vol. 35, no. 3, pp. 59–80, 2018.

[15] K. J. R. Liu and B. Wang, *Wireless AI: Wireless Sensing, Positioning, IoT, and Communications*. Cambridge University Press, 2019.

[16] B. Y. Su, K. C. Ho, M. J. Rantz, and M. Skubic, "Doppler radar fall activity detection using the wavelet transform," *IEEE Transactions on Biomedical Engineering*, vol. 62, no. 3, pp. 865–875, 2015.

[17] M. G. Amin, Y. D. Zhang, F. Ahmad, and K. D. Ho, "Radar signal processing for elderly fall detection: The future for in-home monitoring," *IEEE Signal Processing Magazine*, vol. 33, no. 2, pp. 71–80, 2016.

[18] G. Mokhtari, Q. Zhang, and A. Fazlollahi, "Non-wearable uwb sensor to detect falls in smart home environment," in *2017 IEEE International Conference on Pervasive Computing and Communications Workshops (PerCom Workshops)*, pp. 274–278, 2017.

[19] L. Ma, M. Liu, N. Wang, L. Wang, Y. Yang, and H. Wang, "Room-level fall detection based on ultra-wideband (uwb) monostatic radar and convolutional long short-term memory (lstm)," *Sensors*, vol. 20, no. 4, p. 1105, 2020.

[20] Y. Wang, K. Wu, and L. M. Ni, "Wifall: Device-free fall detection by wireless networks," *IEEE Transactions on Mobile Computing*, vol. 16, no. 2, pp. 581–594, 2016.

[21] H. Wang, D. Zhang, Y. Wang, J. Ma, Y. Wang, and S. Li, "Rt-fall: A real-time and contactless fall detection system with commodity wifi devices," *IEEE Transactions on Mobile Computing*, vol. 16, no. 2, pp. 511–526, 2017.

[22] S. Palipana, D. Rojas, P. Agrawal, and D. Pesch, "Falldefi: Ubiquitous fall detection using commodity wi-fi devices," *Proceedings of the ACM on Interactive, Mobile, Wearable and Ubiquitous Technologies*, vol. 1, no. 4, p. 155, 2018.

[23] L. Zhang, Z. Wang, and L. Yang, "Commercial wi-fi based fall detection with environment influence mitigation," in *2019 16th Annual IEEE International Conference on Sensing, Communication, and Networking (SECON)*, pp. 1–9, 2019.

[24] F. Zhang, C. Chen, B. Wang, and K. J. R. Liu, "Wispeed: A statistical electromagnetic approach for device-free indoor speed estimation," *IEEE Internet of Things Journal*, vol. 5, no. 3, pp. 2163–2177, 2018.

[25] M. A. Al Hafiz Khan, R. Kukkapalli, P. Waradpande, S. Kulandaivel, N. Banerjee, N. Roy, and R. Robucci, "Ram: Radar-based activity monitor," in *IEEE INFOCOM 2016 - The 35th Annual IEEE International Conference on Computer Communications*, pp. 1–9, 2016.

[26] M. S. Seyfioğlu, A. M. Özbayoğlu, and S. Z. Gürbüz, "Deep convolutional autoencoder for radar-based classification of similar aided and unaided human activities," *IEEE Transactions on Aerospace and Electronic Systems*, vol. 54, no. 4, pp. 1709–1723, 2018.

[27] S. D. Regani, C. Wu, B. Wang, M. Wu, and K. J. R. Liu, "mmwrite: Passive handwriting tracking using a single millimeter-wave radio," *IEEE Internet of Things Journal*, vol. 8, no. 17, pp. 13291–13305, 2021.

[28] Y. Gu, F. Ren, and J. Li, "Paws: Passive human activity recognition based on wifi ambient signals," *IEEE Internet of Things Journal*, vol. 3, no. 5, pp. 796–805, 2015.

[29] S. Sigg, U. Blanke, and G. Tröster, "The telepathic phone: Frictionless activity recognition from wifi-rssi," in *2014 IEEE International Conference on Pervasive Computing and Communications (PerCom)*, pp. 148–155, 2014.

[30] S. Kianoush, S. Savazzi, F. Vicentini, V. Rampa, and M. Giussani, "Device-free rf human body fall detection and localization in industrial workplaces," *IEEE Internet of Things Journal*, vol. 4, no. 2, pp. 351–362, 2017.

[31] S. Arshad, C. Feng, Y. Liu, Y. Hu, R. Yu, S. Zhou, and H. Li, "Wi-chase: A wifi based human activity recognition system for sensorless environments," in *2017 IEEE 18th International Symposium on A World of Wireless, Mobile and Multimedia Networks (WoWMoM)*, pp. 1–6, IEEE, 2017.

[32] W. Wang, A. X. Liu, M. Shahzad, K. Ling, and S. Lu, "Device-free human activity recognition using commercial wifi devices," *IEEE Journal on Selected Areas in Communications*, vol. 35, no. 5, pp. 1118–1131, 2017.

[33] Q. Xu, Y. Chen, B. Wang, and K. J. R. Liu, "Trieds: Wireless events detection through the wall," *IEEE Internet of Things Journal*, vol. 4, no. 3, pp. 723–735, 2017.

[34] Q. Chen, B. Tan, K. Chetty, and K. Woodbridge, "Activity recognition based on micro-doppler signature with in-home wi-fi," in *2016 IEEE 18th International Conference on e-Health Networking, Applications and Services (Healthcom)*, pp. 1–6, 2016.

[35] K. Chetty, G. E. Smith, and K. Woodbridge, "Through-the-wall sensing of personnel using passive bistatic wifi radar at standoff distances," *IEEE Transactions on Geoscience and Remote Sensing*, vol. 50, no. 4, pp. 1218–1226, 2012.

[36] W. Li, R. J. Piechocki, K. Woodbridge, C. Tang, and K. Chetty, "Passive wifi radar for human sensing using a stand-alone access point," *IEEE Transactions on Geoscience and Remote Sensing*, pp. 1–13, 2020.

[37] Y. Kim and B. Toomajian, "Hand gesture recognition using micro-doppler signatures with convolutional neural network," *IEEE Access*, vol. 4, pp. 7125–7130, 2016.

[38] S. Björklund, H. Petersson, A. Nezirovic, M. B. Guldogan, and F. Gustafsson, "Millimeter-wave radar micro-doppler signatures of human motion," in *2011 12th International Radar Symposium (IRS)*, pp. 167–174, 2011.

[39] M. Raja, Z. Vali, S. Palipana, D. G. Michelson, and S. Sigg, "3d head motion detection using millimeter-wave doppler radar," *IEEE Access*, vol. 8, pp. 32321–32331, 2020.

[40] Y. Tian, G.-H. Lee, H. He, C.-Y. Hsu, and D. Katabi, "Rf-based fall monitoring using convolutional neural networks," *Proceedings of the ACM on Interactive, Mobile, Wearable and Ubiquitous Technologies*, vol. 2, no. 3, pp. 1–24, 2018.

[41] C. Wu, F. Zhang, and Y. H. K. J. R. Liu, "Gaitway: Monitoring and recognizing gait speed through the walls," *IEEE Transactions on Mobile Computing*, 2020.

[42] Z. Yang, Z. Zhou, and Y. Liu, "From rssi to csi: Indoor localization via channel response," *ACM Computing Surveys (CSUR)*, vol. 46, no. 2, pp. 1–32, 2013.

[43] R. Ramezani, Y. Xiao, and A. Naeim, "Sensing-fi: Wi-fi csi and accelerometer fusion system for fall detection," in *2018 IEEE EMBS International Conference on Biomedical Health Informatics (BHI)*, pp. 402–405, 2018.

[44] Y. Hu, F. Zhang, C. Wu, B. Wang, and K. J. R. Liu, "A wifi-based passive fall detection system," in *ICASSP 2020-2020 IEEE International Conference on Acoustics, Speech and Signal Processing (ICASSP)*, pp. 1723–1727, IEEE, 2020.

[45] V. S. Staggs, L. C. Mion, and R. I. Shorr, "Assisted and unassisted falls: Different events, different outcomes, different implications for quality of hospital care," *The Joint Commission Journal on Quality and Patient Safety*, vol. 40, no. 8, pp. 358–364, 2014.

[46] K. Qian, C. Wu, Z. Yang, Y. Liu, and K. Jamieson, "Widar: Decimeter-level passive tracking via velocity monitoring with commodity wi-fi," in *Proceedings of the 18th ACM International Symposium on Mobile Ad Hoc Networking and Computing*, p. 6, ACM, 2017.

[47] X. Li, D. Zhang, Q. Lv, J. Xiong, S. Li, Y. Zhang, and H. Mei, "Indotrack: Device-free indoor human tracking with commodity wi-fi," *Proc. ACM Interact. Mob. Wearable Ubiquitous Technol.*, vol. 1, Sept. 2017.

[48] K. Qian, C. Wu, Y. Zhang, G. Zhang, Z. Yang, and Y. Liu, "Widar2.0: Passive human tracking with a single wi-fi link," in *Proceedings of the 16th Annual International Conference on Mobile Systems, Applications, and Services*, MobiSys '18, (New York, NY, USA), p. 350–361, Association for Computing Machinery, 2018.

[49] C. Chen, Y. Chen, Y. Han, H.-Q. Lai, F. Zhang, and K. J. R. Liu, "Achieving centimeter-accuracy indoor localization on wifi platforms: A multi-antenna approach," *IEEE Internet of Things Journal*, vol. 4, no. 1, pp. 122–134, 2017.

[50] D. A. Hill, *Electromagnetic fields in cavities: deterministic and statistical theories*, vol. 35. John Wiley & Sons, 2009.
[51] F. Zhang, C. Wu, B. Wang, H.-Q. Lai, Y. Han, and K. J. R. Liu, "Widetect: Robust motion detection with a statistical electromagnetic model," *Proceedings of the ACM on Interactive, Mobile, Wearable and Ubiquitous Technologies*, vol. 3, no. 3, pp. 1–24, 2019.
[52] H. Sakoe and S. Chiba, "Dynamic programming algorithm optimization for spoken word recognition," *IEEE transactions on acoustics, speech, and signal processing*, vol. 26, no. 1, pp. 43–49, 1978.
[53] A. Muscariello, G. Gravier, and F. Bimbot, "Variability tolerant audio motif discovery," in *International Conference on Multimedia Modeling*, pp. 275–286, Springer, 2009.
[54] F. Petitjean, A. Ketterlin, and P. Gançarski, "A global averaging method for dynamic time warping, with applications to clustering," *Pattern Recognition*, vol. 44, no. 3, pp. 678–693, 2011.
[55] F. Petitjean, G. Forestier, G. I. Webb, A. E. Nicholson, Y. Chen, and E. Keogh, "Dynamic time warping averaging of time series allows faster and more accurate classification," in *2014 IEEE International Conference on Data Mining*, pp. 470–479, 2014.
[56] D. Halperin, W. Hu, A. Sheth, and D. Wetherall, "Tool release: Gathering 802.11n traces with channel state information," *SIGCOMM Comput. Commun. Rev.*, vol. 41, p. 53, Jan. 2011.